Analytic Hysteretic Model of Reinforced Concrete Members

철근콘크리트 부재의 해석적 이력모델

정 영 수*
Chung, Young Soo

요 지

지진하중과 유사한 반복하중에 의한 철근 콘크리트 부재의 실제 거동을 재생키 위한 해석적인 이력모델을 제시하였다. 특히 RC부재의 동적거동의 중요한 현상들인 강성저하, 강도저하 그리고 전단영향등의 해석 모델을 소개하였으며 제안된 이력모델의 정확성 및 사용성등의 평가를 위하여 실험결과의 하중 -변위 곡선들과 비교 분석하였다.

ABSTRACT

A mathematical hysteretic model has been developed to analytically reproduce the experimental hysteretic behavior of reinforced concrete members. This mode[2, 3] can simulate the nonlinear response of reinforced concrete members with sufficient accuacy, which are characterized by followng important hysteretic behaviors : stiffness degradation, strength deterioration and shear effect. In order to illustrate the capabilities of the proposed mathematical model, numerical examples are presented with the reproduction of experimental hysteretic behavior of RC members and frames.

1. Introduction

The accurate prediction of the nonlinear behavior of reinforced concrete frames subjected to seismic loading requires a mathematical model of reinforced concrete frame members. In this paper, the model of Roufaiel and Meyer[9] is presented, together with various enhancements. This model takes into account the finite size of the plastic regions and considers the effect of stiffness degradation, strength deterioration, shear and axial forces. A significant improvement is the way in which strength deterioration is sumulated, which is assumed to commence with the first exceedance of the yield moment and accelerates with each inelastic loading cycle in proportion to the amount by which the yield deformation is being exceeded.

* 정회원,중앙대학교 건설대학 토목과 조교수

이 논문에 대한 토론은 1991년 6월 30일까지 본 학회에 보내주시면 1991년 12월호에 그 결과를 게재하겠습니다.

This model leads to analytical response predictions, which compare very well with experimental results and therefore can be considered to be better suited for seismic response calculation than other previously proposed models[4]. In addition, this model also gives an effective tool to develop an advanced seismic design method for RC structures.

2. Material Constitutive Laws

2.1 Concrete

It is well known that concrete exhibits different behavior in tension and compression. The tensile strength can be ignored under seismic loading, because most of it is lost due to cracks caused by service loads. The stress-strain curve for plain concrete has been idealized by many researchers. Herein, Roufaiel and Meyer's refined curve[9] has been adopted with some minor modifications, Fig 1. It is fully described by specifying the following parameters, $f_{cu}=\alpha_c f'_c$, $f_{cy}=\frac{3}{4}f_{cu}$, $\varepsilon_{cu}=\alpha_c\varepsilon_0$, $\varepsilon_{cy}=\frac{5}{12}\varepsilon_{cu}$, and $\varepsilon_{cm}=\beta_c\varepsilon_{cu}$ where f'_c is the uniaxial strength of concrete, ε_0 is the strain at f'_c and ε_{cm} is the critical strain, at which the concrete cover can be observed to spall off, and which can be correlated to the onset of failure. Factors α_c and β_c reflect the confining effect of transverse steel on concrete strength and critical strain, respectively. According to [9], $\alpha_c=1+10\rho''$ and $\beta_c=2+600\rho''$ where $\rho''=\frac{2(b''+d'')A_v}{b''d''S}$ is the volumetric confinement steel ratio, b'' and d'' are the width and depth of the confined core, A_v is the cross sectional area of transverse steel and s is the spacing of transverse steel. The stiffnesses of the three branches of the stress-strain curve of Fig 1 follow as

$$E_c=\frac{f_{cy}}{\varepsilon_{cy}}=\frac{1.8f_{cu}}{\varepsilon_{cu}},\quad P_cE_c=\frac{5}{21}E_c$$

and $$-\bar{P}_cE_c=\frac{f_{cu}-0.1f'_c}{\varepsilon_{cu}-\varepsilon_{cm}}$$

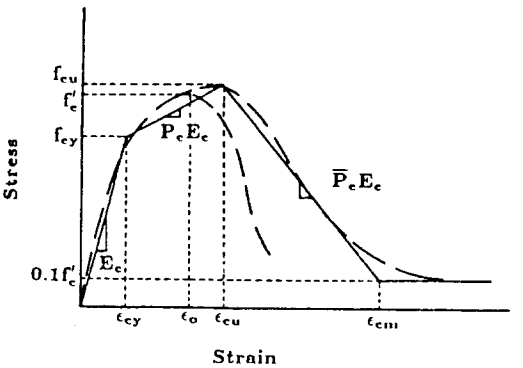

Fig 1. Idealized Stress-Strain Curve of Concrete

2.2 Tensile Reinforcing Steel

Stress-strain curves of steel bars used in reinforced concrete construction are typically idealized as bilinear curves, Fig 2, characterized by Young's modulus, $E_s=\frac{f_{sy}}{\varepsilon_{sy}}$ for the elastic part, and by the strain hardening parameter, $P_s=\frac{1}{E_s}\cdot\frac{f_{su}-f_{sy}}{\varepsilon_{su}-\varepsilon_{sy}}$ for the inelastic part, where f_{sy}=yield strength, f_{su}=ultimate strength, ε_{sy}=yield strain and ε_{su}=ultimate strain. The

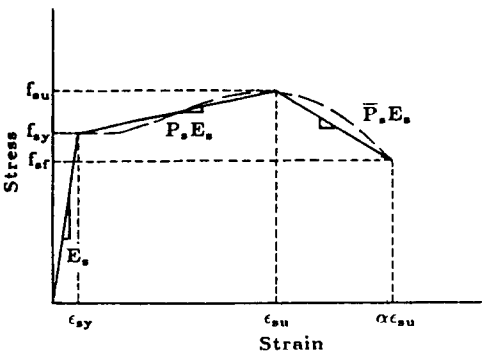

Fig 2. Idealized Stress-Strain Curve of Tensile Steel

unloading branch can be represented by a third linear branch with the negative slope, $-\bar{P}_sE_s = -\gamma P_sE_s$, where can be determined from experimental test data for reinforcing steels. In this analysis, $\gamma = 2.0$ is used.

The descending branch of the stress-strain curve has a significance only for the material point undergoing failure. In a real reinforcing bar, strain localization leads to failure as soon as $\varepsilon_s = \varepsilon_{su}$ is reached. However, in order to facilitate our strength deterioration model for individual members as well as entire frames, it is important that the strain-softening branch of the material stress-strain law be included in the model. Thus it is assumed in the primary moment-curvature relationship that failure is initiated when $\varepsilon_s = \varepsilon_{su}$ and is complete when $\varepsilon_s = \alpha\varepsilon_{su}$. The value of α can be determined in tensile tests of reinforcing bars and is here assumed to be equal to 1.5.

2.3 Compressive Reinforcing Steel

The stess-strain curve for steel in compression is similar to that in tension, provided buckling is prevented. In the light of this restriction it is very rare that steel components in compression enter the strain hardening range. In reinforced concrete members, compression bars are restrained against buckling, as long as the concrete cover has not spalled off. The accurate determination of the buckling stress is very difficult. Herein, it is assumed that the bars canot buckle before they are strained to the point at which the concrete cover spalls off.

3. Primary Moment-Curvature Relationship

The primary moment-curvature curve relates moments to curvatures for monotonic loading. It can be idealized by three linear branches, Fig 3, one for the elastic loading part, one for the inelastic(strain bardening) loading part, and one for the unloading part. Once the stress-strain laws for steel and concrete are specified and the cross-sectional dimensions are known, it is relatively straightforward to compute the moment associated with any specified curvature.

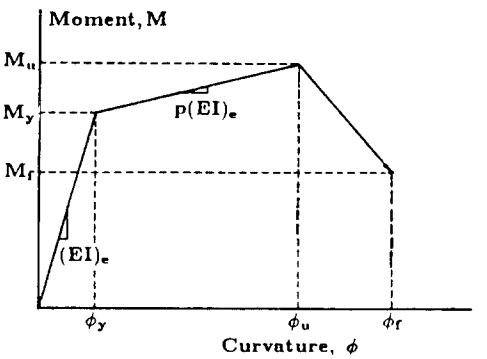

Fig 3. Primary Moment-Curvature Curve

3.1 Neutral Axis and Curvature

If either the concrete strain or the tensile steel strain is assumed, the neutral axis position can be determined for a given moment or curvature by iteration[2]. Assuming that 1) the tensile strength of concrete is ignored, 2) plane sections remain plane after deformation and 3) the axial force, if any, is acting at the plastic centroid, equilibrium of all axial forces acting on the section requires that

$$C_c + C_{s_c} - T_{s_t} - P = 0 \qquad (1)$$

where C_c = compression force in concrete, C_{s_c} = force in compression steel, T_{s_t} = force in the tensile steel and P = external axial force. All of these quantities can be expressed in terms of $\bar{y}$, which is the distance from the compression face to the neutral axis, as $\alpha\bar{y}^2 + \beta\bar{y} - \gamma = 0$ where $\alpha = \alpha_c + \alpha_{s_c} + \alpha_{s_t} + \alpha_p, \beta = \beta_c + \beta_{s_c} + \beta_{s_t} + \beta_p$ and $\gamma =$

$\gamma_c+\gamma_{s_c}+\gamma_{s_t}+\gamma_p$. In these equations, the subscripts c, s_c, s_t and p denote the contributions of concrete, compressive steel, tensile steel and axial force, respectively. The individual terms are tabulated in Tables 1−4 as functions of ε_c. The correct location of the neutral axis can be computed by iteration[2]. Then, the curvature follows as $\phi=\varepsilon_c/\bar{y}$.

Table 1. Coefficients for Concrete Contribution to the Neutral Axis Equation in terms of ε_c

ε_c	α_c	β_c	γ_c
$\leqq\varepsilon_{cy}$	$\frac{1}{2}B$	0.0	0.0
ε_{cy} $\leqq\varepsilon_{cu}$	$\frac{1}{2}B[1-(1-P_c)(1-\frac{\varepsilon_{cy}}{\varepsilon_c})^2]$	0.0	0.0
$>\varepsilon_{cu}$ $\leqq\varepsilon_{cm}$	$\frac{1}{2}B[1-(1-P_c)(1-\frac{\varepsilon_{cy}}{\varepsilon_c})^2$ $-(P_c+P_c)(1-\frac{\varepsilon_{cu}}{\varepsilon_c})^2]$	0.0	0.0
$>\varepsilon_{cm}$	$\frac{1}{2}B[1-(1-P_c)(1-\frac{\varepsilon_{cy}}{\varepsilon_c})^2$ $-(P_c+P_c)(1-\frac{\varepsilon_{cy}}{\varepsilon_c})^2+P_c(1-\frac{\varepsilon_{cm}}{\varepsilon_c})^2]$	0.0	0.0

Table 2. Coefficients for Tensile Steel Contribution to the Neutral Axis Equation in terms of ε_c

ε_s	α_{st}	β_{st}	γ_{st}
$\leqq\varepsilon_{sy}$	0.0	nA_s	nA_sd
$<\varepsilon_{sy}$ $\leqq\varepsilon_{su}$	0.0	$nA_s[1-(1-P_s)(1+\frac{\varepsilon_{sy}}{\varepsilon_c})]$	nA_sP_sd
$>\varepsilon_{su}$	0.0	$nA_s[1-(1-P_s)(1+\frac{\varepsilon_{sy}}{\varepsilon_c})$ $-(P_s+P_s)(1+\frac{\varepsilon_{su}}{\varepsilon_c})]$	$-nA_sP_sd$

Table 3. Coefficients for Compressive Steel Contribution to the Neutral Axis Equation in terms of ε_c

ε_{cm}	α_{sc}	β_{sc}	γ_{sc}
$\leqq\varepsilon_{sy}$	0.0	$(n-1)A_s'$	$(n-1)A_s'd'$
$>\varepsilon_{sy}$	0.0	$(n-1)A_s'\frac{\varepsilon_{sy}}{\varepsilon_c}$	0.0

Table 4. Coefficients for Axial Force Contribution to the Neutral Axis Equation in terms of ε_c

α_p	β_p	γ_p
0.0	$-\frac{P}{E_c\varepsilon_c}$	0.0

3.2 Bending Moment

Once the neutral axis is located, moment equilibrium of all forces acting on the cross section can be established with respect to the plastic centroid by summing up the contributions of the concrete, the compression steel, and tension steel[2].

$$M=M_c+M_{s_c}+M_{s_t} \tag{2}$$

The contribution of the concrete to the moment, M_c, can be obtained depending on the magnitude of compressive strain of concrete. Similarly, the contributions of the tensile and compressive steel are $M_{s_t}=T(d-d'')$ and $M_{s_c}=C_{s_c}(d''-d')$, respectively, where d=effective depth of the cross section, d'=distance from the compression face to the center of compression bars and $d''=d-d'$ for summetric section.

Finally, the complete $M-\phi$ curve is then obtained by repeatedly computing the neutral axis, $\bar{y}$, the curvature, ϕ, and the bending moment, M, by increasing the concrete strain (or steel strain ε_s) from zero until any one of the possible failure modes is reached[2].

4. Hysteretic Behavior of Reinforced Concrete

There are considerable differences between RC member behavior under monotonic and cyclic loading. As a result, failure modes that can be specifically excluded under monotonic load application, by following standard design and detailing procedures, may still prevail under cyclic loading. For example, bond failures can be avoided for most cases by properly developing the reinforcing bar forces. However, under repeated load reversals the steel−concrete interface can deteriorate rapidly and thus become the cause of failure.

4.1 Basic Model Features

A number of models have been proposed in the past to represent the hysteretic behavior of RC members. In a Takeda type model, a set of rules is specified, with which it is possible to characterize the hysteretic behavior more realistically than either a bilinear or degrading bilinear formulation. The model of Roufaiel and Meyer utilizes such a set of rules and therefore has been adopted herein, together with certain improvements to better represent stiffness and strength degradation, Fig 4. It is characterized by five different kinds of branch such as 1) Elastic loading and unloading : $\Delta M=(EI)_1\Delta\phi$. 2) Inelastic loading : If the moment exceeds the yield mement and is still increasing, the moment−curvature relationship is given by $\Delta M=(EI)_2\Delta\phi$. 3) Inelastic unloading : If the moment decreases after the yield moment has been exceeded, the moment−curvature relationship becomes $\Delta M=(EI)_3\Delta\phi$. 4) Inelastic reloading during closing of cracks : In a reversed load cycle, previously opened cracks tend to close, leading to an increase in stiffness and a characteristic "pinched" shape of the moment−curvature curve. This effect is a function of the shear span. If the absolute value of the moment increases but is still less than a certain "crack−closing moment", M_p^+, the moment−curvature relationship is $\Delta M=(EI)_4\Delta\phi$.5) Inelastic reloading after closing of cracks : Once the absolute value of the moment exceeds the " crack−closing moment", M_p^+, and is still increasing, then the moment−curvature relationship is $\Delta M=(EI)_5\Delta\phi$.

4.2 Stiffness Degradation

If the tensile reinforcement is strained beyond the yield point, then the bending stiffness drops from $(EI)_e$ to $p(EI)_e$, Fig 5, where "p" denotes

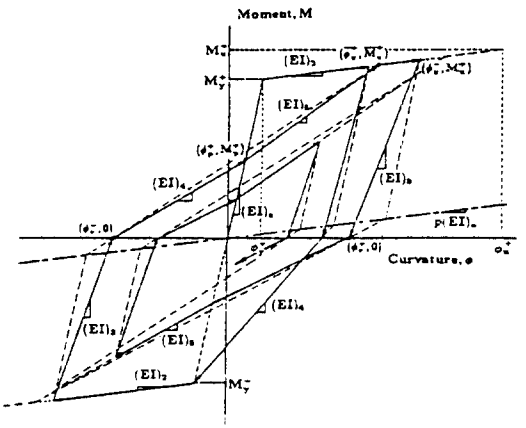

Fig 4. Typical Hysteretic Moment−Curvature Curve

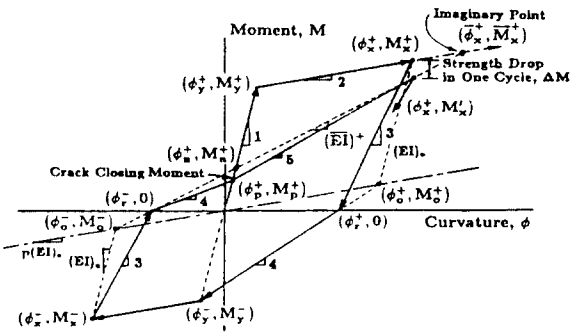

Fig 5. Typical Crack−Closing Moment and Strength Drop

the strain hardening ratio. Upon unloading, the bending stiffness is restored to a value somewhat less than the elastic stiffness, $(EI)_e$. The amount of stiffness degradation is proportional to the maximum displacement. To predict the bending stiffness associated with unloading from a curvature level ϕ (branch 3, Fig 5), one method is to employ a function of the form of $(EI)_3=(EI)_e(\frac{\delta}{\delta_y})$, where β is an empirical constant varying between 0.3 and 0.6, independent of the load history[1]. Atalay and Penzien used the expression $(EI)_3=\alpha K_{cr}$, where $K_{cr}=\frac{F_{max}/F_y}{\delta_{max}/\delta_y}$ is the cracking stiffness, and α is a degradation factor and a function of absolute maximum

displacement. An alternative method is basically graphic. An auxiliary point(ϕ_0^-, M_0^-) is constructed as the point of intersection between a straight line of slope $p(EI)_e$ passing through the origin and a straight line of slope $(EI)_e$ passing through the point of minimum loading, (ϕ_x^-, M_x^-), Fig 5. The residual curvature associated with zero bending moment, ϕ_r^-, is determined by connecting point (ϕ_0^-, M_0^-) with the point of actual maximum loading the opposite direction, (ϕ_x^+, M_x^+). It is debatable whether the slope of the above auxiliary line passing through the origin should be equal to $p(EI)_e$ as proposed by earlier investigators. Since it appears to give realistic results, it is retained herein. Thus, the bending stiffness is $(EI)_3 = \frac{M_x^-}{\phi_x^- - \phi_r^-}$ and according to Fig 5, $M_0^- = \frac{p}{1-p}(\phi_x^-(EI)_e - M_x^-)$, $\phi_0^- = \frac{M_0^-}{p(EI)_e}$ and $\phi_r^- = \phi_0^- - \frac{M_0^-}{(\overline{EI})^+}$ when $(\overline{EI})^+ = \frac{M_x^- - M_0^-}{\phi_x^+ - \phi_0^-}$.

The Bauschinger effect is reproduced by branch 4 in Fig 5, the slope of which is considerably less that of the unloading branch 3. It is determined by connecting the point (ϕ_r^-, 0) with the yield point, or the previous imaginary maximum loading point (ϕ_x^+, M_x^+), in the opposite direction.

4.3 Shear Effect on Hysteretic Behavior

The effect of shear has been investigated by many researchers[1, 5, 6, 8]. When load reversal occurs within the inelastic range in the presence of high shear, the open shear cracks will initially permit the transfer of shear forces mostly through dowel action only, leading to a rather low stiffness. After the closing of such cracks, aggregate interlock and shear friction cause a significant increase of the member stiffness. Roufaiel has modeled this effect by intorducing the "crack-closing" moment M_p^+, associated with curvature ϕ_p^+, Fig 5. If shear stresses are negligible and the hysteresis loops are stable during cyclic loading, no pinching is likely to occur and branches 4 and 5 will form a single straight line. In this case, the point (ϕ_p^+, M_p^+), will degenerate to a "point to no pinching", with the following corrdinates (Fig 5):

$$\phi_n^+ = \phi_r^- \frac{(\overline{EI})}{(\overline{EI}) - (EI)_e} \qquad M_n = (EI)_e \phi_n$$

$$\text{when } (\overline{EI}) = \frac{M_x^-}{\phi_x^- - \phi_r^-} \tag{3}$$

A "pinching factor" α_p, is now introduced such that $\alpha_p = 1$, if the shear effect is negligible, and $\alpha_p = 0$, if the shear effect completely controls the load-deformation behavion. The coordinates of the "crack-closing" point can be expressed as $M_p^+ = \alpha_p M_n^+$ and $\phi_p^+ = \alpha_p \phi_n^+$, where $\alpha_p = 0$ if $\frac{a}{d} \leq 1.5$, $\alpha_p = \sqrt{0.4 \quad -0.6}$ if $1.5 < \frac{a}{d} \leq 4.0$ and $\alpha_p = 1$ if $\frac{a}{d} > 4$. Details are given in Ref[2].

4.4 Strength Deterioration

In addition to stiffness degradation, RC members experience strength deterioration under cyclic loading beyond the yield level. The rate of strength deterioration and the failure curvature depend on many factors, such as the confinement ratio, axial force, concrete strength etc. If the failure curvature for monotonic loading is known, it is possible to derive a strength deterioration curve, as will be shown below. Atalay and Penzien[1] had noticed some correlation between commencement of strength deteroration and the spalling of the concrete cover. But Hwang's experiments[6] showed that

strength deterioration can start at considerably lower load levels. Even for loads slightly above the yield level, damage and strength deterioration can be observed, provided a sufficiently large number of load cycles is applied. Roufaiel[9] found a strong correlation between the onset of strength deterioration and a "critical" displacement level, at which the concrete in the extreme compression fibre is strained to some limit value. More significantly, it is unreasonable to stipulate such a precisely defined point of failure initiation, i.e. to say if this point is exceeded by a small amount, strength deterioration is initiated, but if it is missed by a small amount, no such strength deterioration takes place. It is, therefore, suggested that strength deterioration is initiated as soon as the yield load level is exceeded, and the strength deterioration accelerates as the critical load level is reached. For this purpose, a strength drop index, S_d, is proposed which defines the strength drop to be expected for a given curvature, ϕ, in a single load cycle(Fig 6).

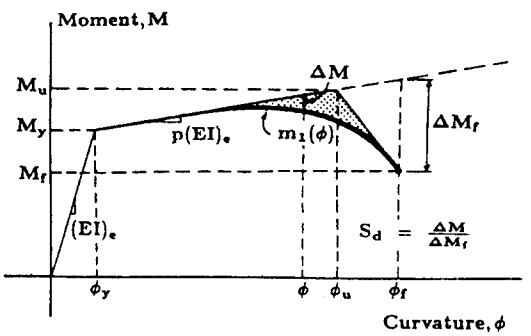

Fig 6. Strength Deterioration Curve

$$S_d=\frac{\Delta M}{\Delta M_f}=A\left[(\frac{\phi}{\phi_{ur}})^{2\omega}+B(\frac{\phi}{\phi_u})^{\omega}+C\right] \quad (4)$$

where S_d=strength drop index for curvature in a single load cycle, ΔM=moment capacity reduction in a single load cycle up to curvature (ϕ), ΔM_f=moment capacity reduction in a single load cycle up to failure curvature(ϕ_f), ϕ_u= curvature corresponding to ultimate moment capacity(M_u), and A, B, C, ω are free constants. With ΔM denoting the strength drop in the first subsequent load cycle for some curvature ϕ, the residual strength after this load cycle is given by $m_1(\phi)=M(\phi)-S_d\Delta M_f$. Some of the free constants in Eq (4) can be determined from specified boundary conditions : 1) $\Delta M=0$ at $\phi=\phi_y$, i.e. $S_d|_{\phi=\phi_y}=0$, 2) As $m_1(\phi)$ is tangent to the inelastic loding branch at $\phi=\phi_y$, i.e. $\frac{dm_1}{d\phi}=p(EI)_e$, it follows that $\frac{dS_d}{d\phi}\Big|_{\phi=\phi_y}=0$ and 3) $m_1=M_f$ at $\phi=\phi_f$. Using specified boundary conditions, then, one obtains $S_d=(\frac{\phi-\phi_y}{\phi_f-\phi_y})^{\omega}$. Finally, the residual strength after the first subsequent load cycle is

$$m_1(\phi)=M_y+(\phi-\phi_y)p(EI)_e-\Delta M \quad (5)$$

where $\Delta M=[(\phi_f-\phi_y)p(EI)_e+M_y-M_f](\frac{\phi-\phi_y}{\phi_f-\phi_y})^{\omega}$. On the basis of selected experimental data, a value for of 1.5 appears to five good results.

In order to incorporate this concept of strength deterioration into the hysteresis model, the coordinates of the imaginary point become

$$\bar{\phi}_x=\frac{1}{(\overline{EI})-p(EI)_e}[M_y-\bar{M}_0-\phi_y p(EI)_e+\bar{\phi}_0(\overline{EI})]$$

$$\bar{M}_x=\bar{M}_0+\frac{(\overline{EI})}{(\overline{EI})-p(EI)_e}[M_y-\bar{M}_0+(\bar{\phi}_0-\phi_y)p(EI)_e] \quad (6)$$

where $(\overline{EI})=\frac{M'_x-\bar{M}_0}{\phi_x-\bar{\phi}_0}$ and $M'_x=M_x-\Delta M$. In these equations, the superscripts, "+" and "−", denote loading in the positive and negative sense, respectively.

5. Implementation and Numerical Examples

The hysteretic model has been also incorporated into the computer program, SARCF(Seismic Analysis of Reinforced Concrete Frames), which has been coded by Chung et al[4]. To illustrate the accuracy, with which the model can simulate hysteretic response of RC members, some numerical examples will be presented below. These cases were selected from a number of simulation studies because they exhibited pronounced strength drops under constant amplitude loading, in which case the model's capacity to simulate strength deterioration is challenged most. For this purpose, Hwang's experiment[6], some of the Berkeley tests[5, 8] and Ohno's tests[7] appeared to be most appropriate. To realistically simulate cyclic behavior of RC members, mathematical hysteretic models must consider the effect of strength deterioration, which can be clearly noticed in low cycle fatigue tests.

5.1 Basic Simulation Procedure

Since most of the laboratory experiments to be simulated numerically were displacement controlled and of quasi-static nature, the effects of inertia and damping were ignored in the analysis. Then, the nonlinear equations of motion reduce to $[K]\{\Delta X\}=\{\Delta P\}$ where $[K]$ = tangent stiffness matrix, $\{\Delta X\}$ = displacement increment vector, and $\{\Delta P\}$ = load increment vector. The equations can be partitioned as:

$$\begin{bmatrix} K_{ff} & K_{ss} \\ K_{sf} & K_{ss} \end{bmatrix} \begin{Bmatrix} \Delta X_f \\ \Delta X_s \end{Bmatrix} = \begin{Bmatrix} \Delta P_f \\ \Delta P_s \end{Bmatrix} \tag{7}$$

where the subscripts, "s" and "f", respectively, denote those degrees of freedom that are fixed to the supports and those that are not. Because $\{\Delta X_s\}=\{0\}$, the equations simplify as $[K_{ff}]\{\Delta X_f\}=\{\Delta P_f\}$. These equations are again partitioned as:

$$\begin{bmatrix} K_{ffoo} & K_{ffoi} \\ K_{ffio} & K_{ffii} \end{bmatrix} \begin{Bmatrix} \Delta X_{fo} \\ \Delta X_{fi} \end{Bmatrix} = \begin{Bmatrix} \Delta P_{fo} \\ \Delta P_{fi} \end{Bmatrix} \tag{8}$$

where "i" refers to those degrees of freedom for which non-zero displacements are prescribed (in a displacement controlled test), and "o" refers to all other degrees of freedom. With $\{\Delta P_{fo}\}=\{0\}$, Eq (8) leads to $\{\Delta X_{fo}\}=-[K_{ffoo}]^{-1}[K_{ffoi}]\{\Delta X_{fi}\}$ and $([K_{ffii}]-[K_{ffio}][K_{ffoo}]^{-1}[K_{ffoi}])\{\Delta X_{fi}\}=\{\Delta P_{fi}\}$.

Finally, the relationships between $\{\Delta P_{fi}\}$ and $\{\Delta X_{fi}\}$ can be plotted and compared with the corresponding experimental results.

5.2 Result of Numerical Examples

Hwang's experiments[6] explored the relationship between load history and total energy dissipation capacity of RC flexural members. He tested a total of eleven cantilever specimens under displacement control and various load histories. All of these were alalyzed, and agreement between experimental and analytical load deformation curves was good[2]. Two experiments performed at the Unversity at Berkeley (8) have been analyzed to simulate the behavior of the crack-closing moment as well as the strength deterioration of RC members under variable load history. These results are also illustrative of the accuracy with which experimental behavior can be reproduced analytically. In addition, Ohno et al[7] had performed a series of experiment for one bay one story frame model, which was based on constant or few kinds of amplitude of quasi-static controlled displacement, to investigate the energy absorption capacity of RC structures. The reproduction of hysteretic behavior for RC frame model appear to be also by and large accurate. Some

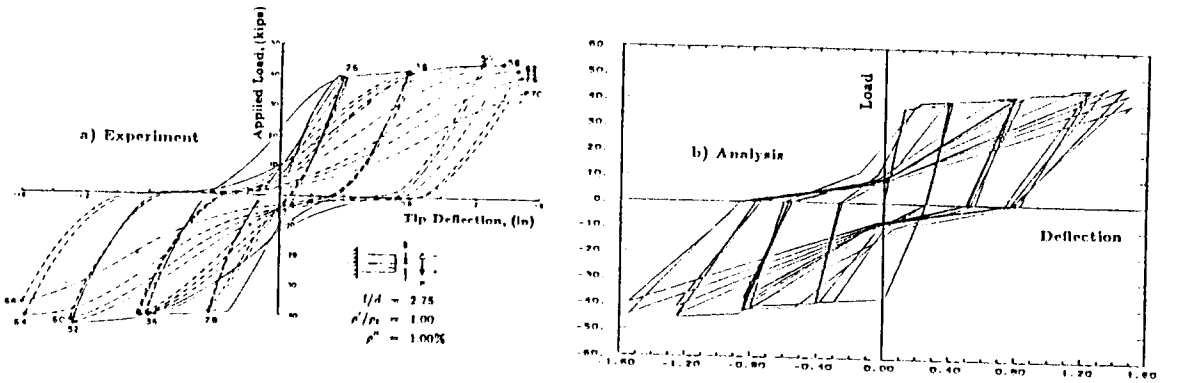

Fig 7. Experimental and Analytic Load–Deformation Curves for Beam R5 Tested by Ma, Bertero and Popov[8]

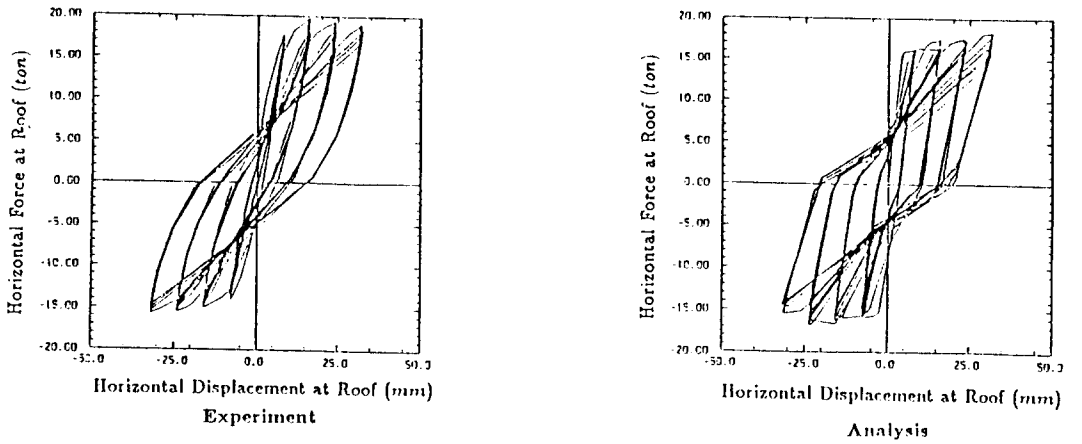

Fig 8. Experimental and Analytic Load–Deformation Curves for Frame No.4 Tested by Fujikake, Ohno and Nishioka [7]

of these numerical simulations are reproduced in Fig 7 and 8. It is, in particular, noted how closely the experimentally observed strength deterioration is reproduced numerically. This is an indication that the damage index to be introduced in for further study, on which this hysteretic model is implicitly based, promises to be reliable.

6. Conclusions

An analytic hysteretic model has been proposed with various enhancements that is believed to be more rational. It is based on a thorough investigation of the many factors that can contribute to the hysteresis of reinforced concrete member subjected to cyclic loadings. Some model parameters were calibrated against the few available experimental results. For example, the rate of strength deterioration and stiffness degradation were thus determined. An accurate reproduction of the experimental load–deformation curve is essential for meaningful nonlinear dynamic analysis of reinforced concrete structure. The principal shortcoming of the model is the limited number of the test data which is based on the quasi–static experiment performed under the constant load amplitude. Thus, available

experimental investigations be undertaken, especially to determine the relationship between load and deformation level and to study the influence of important parameters, such as confinement ratio, longitudinal steel reinforcement ratio, and shear reinforcement.

감사의 글

이 논문은 1990년 문교부학술진흥재단의 자유공모과제 학술연수 조성비에 의하여 연구된 일부임. 이 연구를 지원해주신 관계 제위께 심심한 사의를 표합니다.

References

1) Atalay, M.B. and Penzien, J.,"The Seismic Behavior of Critical Regions of Reinforced Concrete Components as Influenced by Moment, Shear and Axial Forces," Report No. EERC-75-19, Univ. of California at Berkeley, CA, 1975.
2) Chung, Y.S., Meyer, C. and Shinozuka, M., " Seismic Damage Assessment of Reinforced Concrete Members," Report No. NCEER-87-22, National Center for Earthq. Engr. Research, Buffalo, NY, Oct. 1987.
3) Chung, Y.S., Meyer, C. and Shinozuka, M., " Modelling of Concrete Damage," ACI Struct. Journal, Vol.86, No.3, May-Jun. 1989.
4) Chung, Y.S., Meyer, C. and Shinozuka, M., " SARCF User's Guide(Seismic Analysis of Reinforced Concrete Frames)," Report No. NCEER-88-44, National Center for Earthq. Engr. Research, Buffalo, NY, Nov. 1988.
5) Clough, R.W. and Johnston, S.B., "Effect of Stiffness Degradation on Earthquake Ductility Requirements," Proceeding of Japan Earthq. Engr. Symposium, Oct. 1966.
6) Hwang, T.H. and Scribner C.F., "R/C Members Cyclic Response During Various Loading," Journal of Struct. Engr., ASCE, Vol.110, No.3, Mar. 1984.
7) Fujikake, K., Ohno, T. and Nishioka, T., " Experimental Study on Energy Absorption Capacity of Reinforced Concrete Frames," Proceedings of JSCE, No.390, Vol.8, Japan, Feb. 1988.
8) Ma, S-Y. M., Bertero, V.V. and Popov, E.P., "Exoerimental and Analytical Studies on the Hysteretic Behavior of Reinforced Concrete Rectangular and T-Beam," Report No. EERC-76-2, Univ. of California at Berkeley, CA, 1976.
9) Roufaiel, M.S.L. and Meyer, C., "Analytical Modeling of Hysteretic Behavior of R/C Frames," Journal of Struct. Engr., ASCE, Vol.113, No.3, Mar. 1987.

(접수일자 : 1991. 2. 8)